

1 **Recent decrease in summer precipitation over the Iberian Peninsula**
2 **closely links to reduction of local moisture recycling**

3 Yubo Liu^{1,2}, Monica Garcia^{3,4}, Chi Zhang^{1,5}, Qihong Tang^{1,2*}

4

5 ¹Key Laboratory of Water Cycle and Related Land Surface Processes, Institute of Geographic
6 Sciences and Natural Resources Research, Chinese Academy of Sciences, Beijing, China

7 ²University of Chinese Academy of Sciences, Beijing, China

8 ³Research Center for the Management of Environmental and Agricultural Risks (CEIGRAM),
9 E.T.S. de Ingeniería Agronómica, Alimentaria y de Biosistemas, Universidad Politécnica de
10 Madrid, Avda. Senda del Rey, 13, 28040 Madrid, Spain

11 ⁴Sino-Danish Center for Education and Research (SDC), 8000 Aarhus C, Denmark

12 ⁵Key Laboratory of Land Surface Pattern and Simulation, Institute of Geographic Sciences and
13 Natural Resources Research, Chinese Academy of Sciences, Beijing, China

14

15 ***Correspondence:** Qihong Tang (tangqh@igsnr.ac.cn)

16

17 **Abstract**

18 The inherently dry summer climate of the Iberian Peninsula (IP) is undergoing drought
19 exacerbated by more intense warming and reduced precipitation. Although many
20 studies have studied changes in summer climate factors, it is still unclear how the
21 changes in moisture contribution from the sources lead to the decrease in summer
22 precipitation. This study investigates the differences in the IP precipitationshed between
23 1980-1997 and 1998-2019 using the Water Accounting Model-2layers with ERA5 data,
24 and assesses the role of local moisture recycling and external moisture in reducing
25 summer precipitation. Our findings indicate that the moisture contributions from the
26 local IP, and from the west and the east of the precipitationshed contributed 1.7, 3.6 and
27 1.1 mm mon⁻¹ less precipitation after 1997 than before 1997, accounting for 26 %, 57 %
28 and 17 % of the main source supply reduction, respectively. The significant downward
29 trend of the IP local moisture recycling closely links to the disappearance of the wet
30 years after 1997 as well as the decrease of local contribution in the dry years. Moreover,
31 the feedback between the weakened local moisture recycling and the drier land surface
32 can exacerbate the local moisture scarcity and summer drought.

33

34 **1. Introduction**

35 The Iberian Peninsula (IP) is located in the Mediterranean basin, which is among
36 the global “hotspots” of climate change. The IP precipitation is characterized by the
37 diverse climatic regimes and high spatial variability as a consequence of its geographic
38 position between the Atlantic Ocean and the Mediterranean Sea and its orographic
39 configuration. In responding to climate change with frequent heatwaves and above-
40 average warming, the IP is experiencing widespread decreases in precipitation,
41 especially in summer (Brogli et al., 2019; Cramer et al., 2018; Rajczak and Schär, 2017).
42 This reduction in summer precipitation is a major driver of water resource depletion
43 and the evolution of drought (Lopez-Bustins and Lemus-Canovas, 2020; Páscoa et al.,
44 2021; Teuling et al., 2013). To clarify the reason for the decrease in summer
45 precipitation, it is necessary to explain the changes in moisture contribution from the
46 sources, such as local moisture recycling and external sources.

47 Analysis of source supply and transportation in the hydrological cycle has become
48 one efficient way to understand well regional precipitation. With the introduction of the
49 concept of precipitationshed (Keys et al., 2014; Keys et al., 2011), which better reveals
50 the contribution from upwind evaporation sources to the precipitation in downwind sink
51 region, it is more scientific and systematic to explain the precipitation variations by
52 using the fluctuations of moisture contribution as a precursor. Given the importance of
53 studying the source of precipitation, that is, precipitationshed, a variety of methods have
54 been developed and adopted, including physical isotope analysis (Bonne et al., 2014),

55 and numerical analytical models, either online methods running in parallel with climate
56 models (Damián and Gonzalo, 2018; Stohl and James, 2004, 2005), or offline
57 “posteriori models” (van der Ent and Savenije, 2011; van der Ent et al., 2010; van der
58 Ent et al., 2013). Furthermore, the local moisture recycling, which describes the local
59 precipitation-evaporation feedback relationship, has been proposed to further
60 differentiate regional local and external contributions to the designated area. Although
61 the mechanisms of these studies are different, they all emphasize that the constantly
62 changing source-sink relationship of atmospheric moisture is an essential part of
63 climate change research as global change continues.

64 Gimeno et al. (2010) comprehensively investigated the atmospheric moisture
65 sources of the IP precipitation at different scales, and identified the tropical–subtropical
66 North Atlantic corridor, the surrounding Mediterranean Sea and the local IP as
67 important moisture regions. The high precipitation in the cold season is mainly
68 dominated by westerly wind regimes. The mid-latitude atmospheric dynamics, such as
69 the baroclinic synoptic-scale perturbations from the Atlantic and the polar jet stream,
70 as well as the high moisture supply from an Atlantic “tropospheric river” seem to be
71 responsible for the abundant precipitation during the cold season (Cortesi et al., 2013;
72 Ulbrich et al., 2015; Zhu and Newell, 1998). Compared to the rainy winter, the summer
73 with very low precipitation receives less attention. The subtropical location under the
74 descending air extending from the North Atlantic subtropical high controls low summer
75 precipitation over the IP, and local convective events increase the importance of local

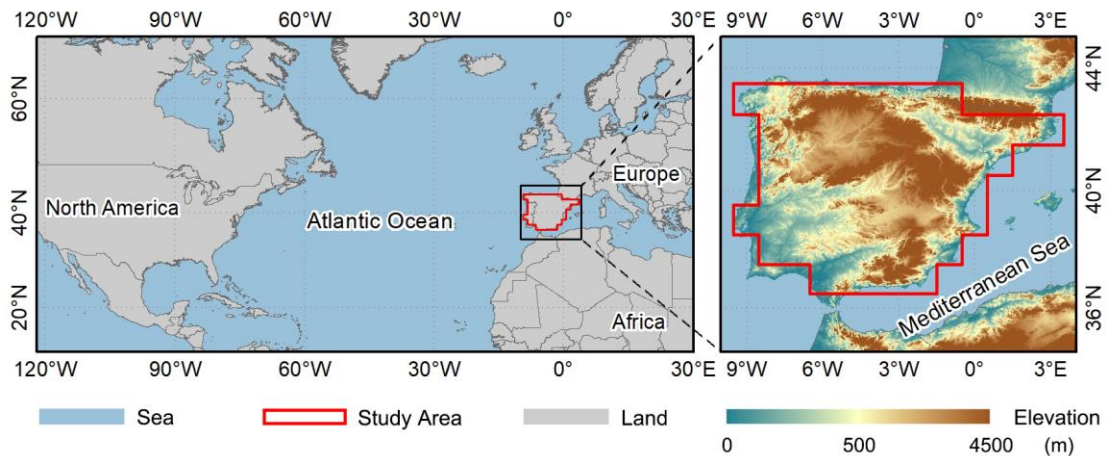
76 moisture recycling during summer (Serrano et al., 1999). Accordingly, the summer IP
77 precipitation, with a significant proportion of the locally recycled moisture, is
78 completely different from the winter IP precipitation that is dominated by the distant
79 external moisture.

80 In recent decades, the increasing severity of summer drought in the IP, which is
81 closely related to precipitation variations, has attracted more attention. Several
82 mechanisms, including soil-atmosphere interactions (Boé and Terray, 2014), cloud
83 processes (Lenderink et al., 2007; Tang et al., 2012) and large-scale circulation changes
84 (Boé et al., 2009; Brogli et al., 2019; Kröner et al., 2017), have been found to be
85 potentially important for this complex summer climate change, which also appear to
86 have an impact on the precipitation reduction. Such anomaly of summer precipitation
87 in the sink is inevitably linked to source changes, but there is still a lack of knowledge
88 about how source moisture contributes to precipitation decline. Therefore, tracing the
89 precipitationshed of the IP and quantifying the moisture contributions can provide us
90 with a new perspective to analyze the changes in IP precipitation. This study aims to
91 evaluate the moisture contribution of the local moisture recycling and external sources
92 to the reduced summer precipitation over the IP. It can provide a scientific reference for
93 the prediction and management of droughts that may be caused by precipitation
94 reduction from the perspective of source moisture contribution.

95 **2. Study Area, Data and Methods**

96 2.1 Study area

97 The IP is located in southwestern Europe at midlatitudes of the northern
98 hemisphere. It covers Portugal and the mainland of Spain. The geographic location of
99 IP is shown in Fig. 1(a) (36°N-44°N, 10°W-3°E) in a transition zone between
100 midlatitude and subtropical atmospheric circulation regimes. It has a complex
101 topography, surrounded by the Atlantic Ocean and Mediterranean Sea, and elevated in
102 the middle and northeast. The topographic and coastal processes affect water vapor
103 transport, forming a spatial precipitation gradient from the northwest to the southeast.
104 Extracted from the land-sea mask provided by European Centre for Medium-range
105 Weather Forecasts (ECMWF), the red outline area composed of multiple single 1×1
106 degree grids is our study area of the IP.



107
108 **Figure 1** Map of the IP (the area within the closure of the red line) on a grid of 1°×1° as the target
109 region.

110

111 2.2Data

112 The newest reanalysis data held in ECMWF data archive, the ERA5 dataset
113 downloaded from the Copernicus Climate Change Service (C3S) Climate Data Store
114 (CDS) is used in this study (Hersbach et al., 2020). The variables include surface
115 pressure, precipitation, evaporation, total column water, and vertical integrated
116 eastward and northward atmospheric water fluxes (including cloud liquid water flux,
117 cloud frozen water flux and water vapor flux) on single level, as well as the horizontal
118 U/V components of wind fields and specific humidity at the lowest 23rd pressure levels
119 (200-1000hPa). The time resolution and spatial resolution selected for these data are 1
120 hour and 1×1 degree, respectively. This dataset covers the period from 1980 to 2019.
121 Compared to the old version reanalysis data (e.g., ERA-Interim or ERA-40), ERA5
122 combines vast amounts of historical observations into global estimates using more
123 advanced modelling and data assimilation systems (Hersbach et al., 2020).

124 As the ERA5 precipitation is a global forecast dataset with some uncertainties, its
125 reliability in the IP region needs to be verified. Therefore, an observational gridded
126 dataset generated from a dense network of stations over the IP, named the Iberia01
127 (Herrera et al., 2019), is used to verify the accuracy of the ERA5 precipitation data. The
128 Iberia01 provides the daily precipitation for the period of 1971-2015 at 0.1×0.1 degree.

129 2.3 Model and methods

130 2.3.1 Water Accounting Model-2layers

131 Water Accounting Model-2layers (WAM-2layers) is an offline Eulerian method
132 tracking the moisture cycle forwards or backwards that quantifies the source-sink
133 relations (van der Ent et al., 2013; van der Ent et al., 2014). Its backward algorithm was
134 used in this study to trace the precipitation shed of the IP. The model of WAM-2layers
135 is an updated version of the original WAM. The water vapor balance equation in the
136 WAM-2layers algorithm maintains the premise that the atmosphere is well mixed, but
137 compared with the previous model, it takes the stratification of the atmosphere into
138 consideration. Thus, when the algorithm is applied to a specific region, the calculation
139 is as follows,

$$140 \quad \frac{\partial W_{l,r}}{\partial t} + \frac{\partial(W_{l,r}u)}{\partial x} + \frac{\partial(W_{l,r}v)}{\partial y} = E_{l,r} - P_{l,r} \pm F_{v,r} + \alpha_{l,r} \quad (1)$$

141 where W is the atmospheric moisture storage, or namely, precipitable water; t is time; u
142 and v are the wind components in x (zonal) and y (meridional) direction, respectively;
143 E is evaporation; P is precipitation; F_V is the vertical moisture transport between the
144 bottom and top layer; α is a residual term, which is resulted from the ERA5 data
145 assimilation and the coarser resolution scheme in the model calculation (van der Ent et
146 al., 2014); the subscript l represents the portion in layer l (either the bottom layer or the
147 top layer), and the subscript r represents the tagged portion provided by the source
148 region.

149 Based on the assumption of a well-mixed atmosphere (Burde, 2010; Goessling and
 150 Reick, 2013), the moisture contribution, that is, the tagged evaporation E_r , can be
 151 calculated considering that the ratio of tagged to total atmospheric water storage is equal
 152 to the ratio of tagged to total evaporation, as shown in Eq. (2). Considering the proposed
 153 retention time of atmospheric moisture is about 1 week to 10 days (Numaguti, 1999),
 154 we set the backtracking time as 1 month longer for summer precipitation to make sure
 155 that more than 90 % of the precipitation can be redistributed to the surface (Zhang et
 156 al., 2017).

$$157 \quad E_r(t, x, y) = E(t, x, y) \frac{W_r(t, x, y)}{W(t, x, y)} \quad (2)$$

158 The main moisture source supplying IP summer precipitation is defined as the 90th
 159 percentile precipitation shed in this study. It is further divided into subregions to
 160 evaluate the role of the contribution from each area, such as the local moisture recycling,
 161 which demonstrates the contribution of local evaporation to the IP precipitation, and
 162 the external advection moisture, which describes the non-local evaporation contribution
 163 to the IP precipitation. The contribution ratio (CR) of a subregion (A) is defined as the
 164 proportion of the moisture contribution from it to the total contribution from the main
 165 source region (MS), which is calculated as the following Eq. (3). The precipitation
 166 recycling ratio of the IP can be substituted with the IP local contribution ratio CR_{IP} .

$$167 \quad CR_A = \frac{\sum E_r(t, x, y|A)}{\sum E_r(t, x, y|MS)} \times 100\% \quad (3)$$

168 2.3.2 Significance test

169 The slope significance of trend fitting and the significance of the difference in the
170 means are tested using Student t-test in this study. Additionally, the moving t-test, as a
171 method of mutation analysis, is used to detect whether and when the sample mean in
172 the IP precipitation series changed significantly. The precipitation series is divided into
173 two non-overlapping adjacent segments of length n years before and after the reference
174 year, to compare changes in the mean (Maasch, 1988),

175
$$T = \frac{(\bar{x}_1 - \bar{x}_2)\sqrt{n}}{\sqrt{S_1^2 + S_2^2}} \quad (4)$$

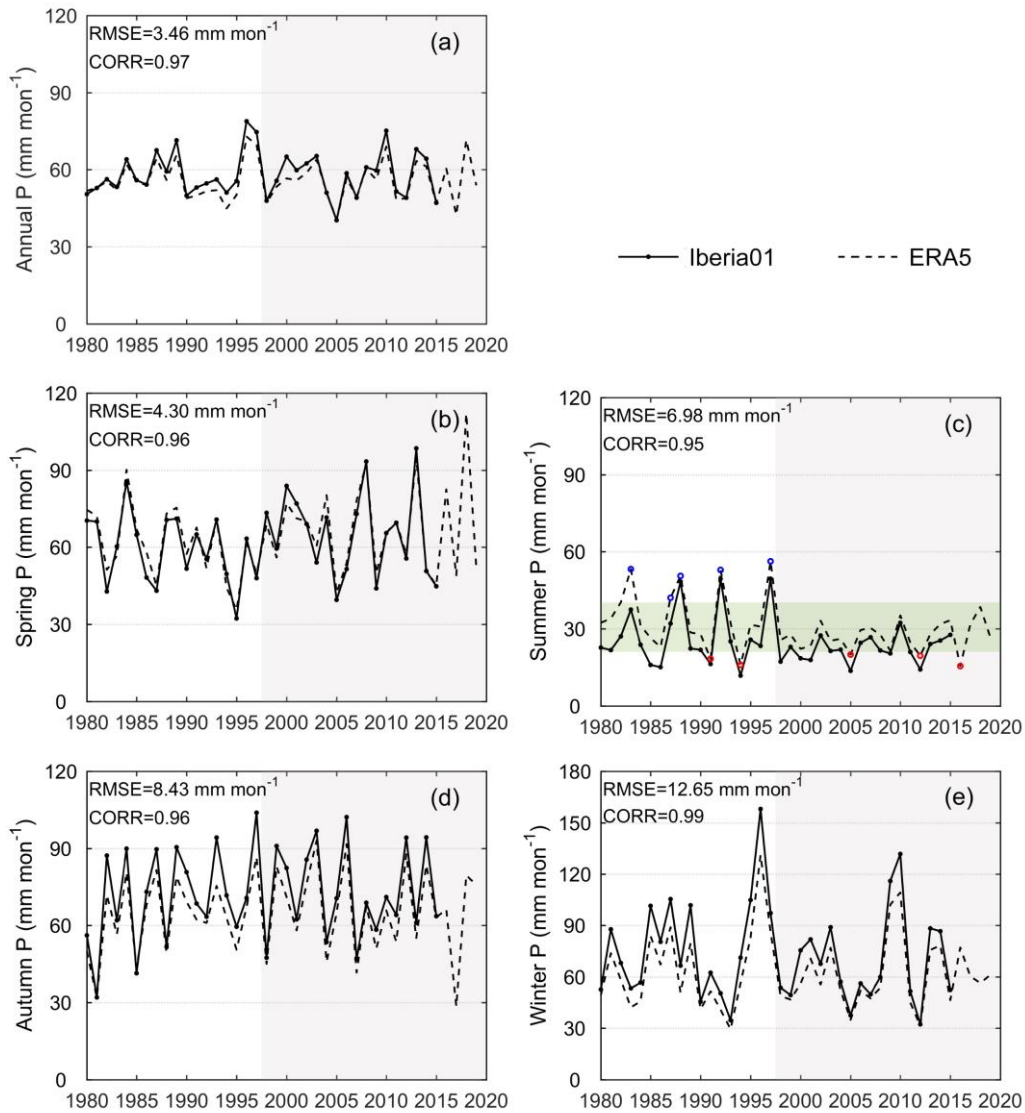
176 where \bar{x}_1 and \bar{x}_2 denote the respective means of two segments, and S_1^2 and S_2^2 are their
177 variances.

178 **3. Results**

179 3.1 Evaluation and variation of precipitation data

180 The precipitation time series of the ERA5 and the Iberia01 data are shown in Fig.
181 2. The fluctuations and variations of the ERA5 precipitation data are in good agreement
182 with the observed data on both annual and seasonal scales, together with all correlation
183 coefficients higher than 0.95. The average annual precipitation over the IP is about
184 55.66 mm mon⁻¹ from ERA5 and 58.07 mm mon⁻¹ from Iberia01, respectively.
185 Compared with the observed data, the reanalysis data slightly underestimates the IP
186 precipitation with the root mean square error (RMSE) of 3.46 mm mon⁻¹ on the annual

187 scale. The comparison of seasonal precipitation shows that the ERA5 is lower than the
188 observed Iberia01 value in the rainy seasons (both winter and autumn), but higher in
189 the dry summer. The RMSE between the two datasets of seasonal precipitation is in the
190 range of 4.30-12.65 mm mon⁻¹. Since the Iberia01 data is the grid data interpolated from
191 observation site data (Herrera et al., 2019), some of the deviations between the ERA5
192 and the Iberia01 precipitation can be partially affected by the interpolation process
193 rather than solely the result of the error generated by the reanalysis process. In general,
194 the ERA5 precipitation data shows the characteristics of IP precipitation reasonably
195 well and thus is suitable for studying the changes.



196

197 **Figure 2** Variations of IP (a) annual precipitation, (b) spring (March, April and May), (c) summer

198 (June, July and August), (d) autumn (September, October and November) and (e) winter (December,

199 January and February) during 1980-2019. The white shading is for the period 1980-1997 and the

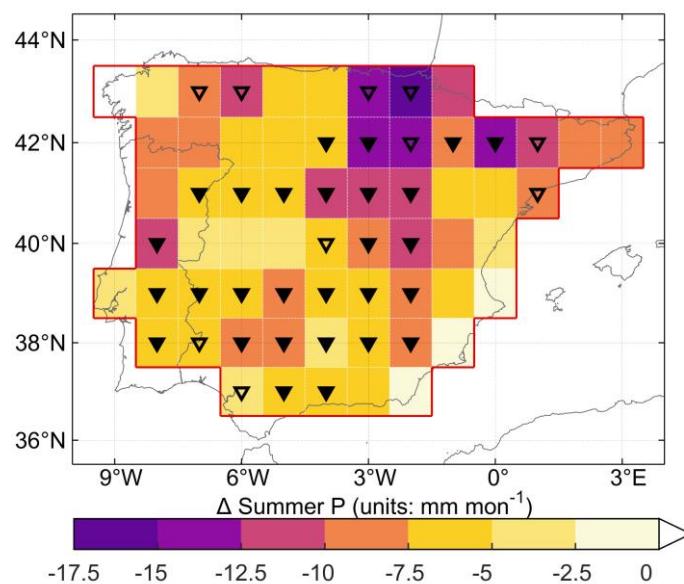
200 grey shading is for the period 1998-2019. The green shading covers the interval of one standard

201 deviation of summer precipitation. The years with summer ERA5 precipitation exceeding the range

202 of the green shading interval are circled in blue and red.

203 Only in summer, the mutation analysis results of the two sets of precipitation data,

204 the Iberia01 (T value: 1.83) and the ERA5 (T value: 1.86), both show statistically
205 significant changes at 0.1 level in the year 1997. Accordingly, the entire 40-year period
206 is divided into two periods, 1980-1997 and 1998-2019, to compare the difference in
207 summer precipitation between the two periods. The average summer precipitation is
208 34.89 and 27.17 mm mon⁻¹ before and after 1997, respectively. Compared with 1980-
209 1997, the average summer precipitation during 1998-2019 decreases by 7.72 mm
210 (22.13 %) in the whole study area. On the grid scale, almost all grids have less
211 precipitation after 1997, and more than half of all grids show the statistically significant
212 reductions (Fig. 3). However, this change is unevenly distributed in space, as shown by
213 the greater reduction in the grids on the northeastern IP that can even exceed 10 mm
214 mon⁻¹.



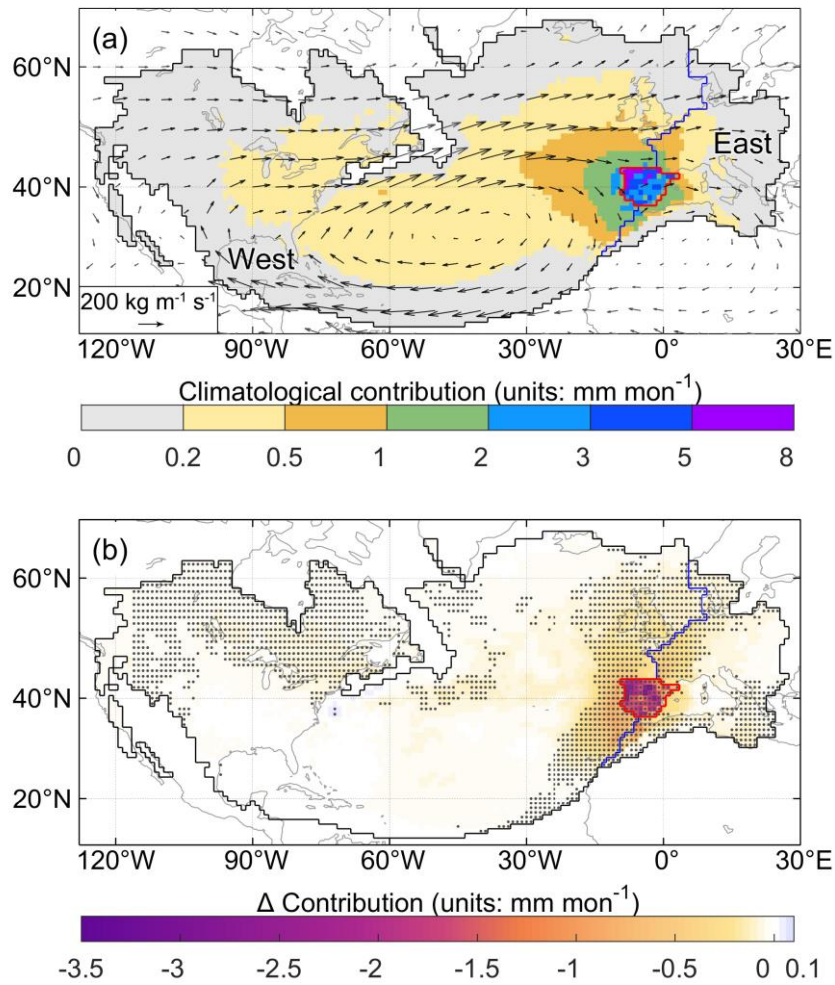
216 **Figure 3** The difference of average summer precipitation over the IP between 1998-2019 and 1980-
217 1997 (average of 1998-2019 minus average of 1980-1997). The triangles indicate that the
218 differences are significant at 0.05 (solid) and 0.1 (hollow) level.

219 For summer precipitation, the dry years (1991, 1994, 2005, 2012 and 2016) and
220 the wet years (1983 1987 1988 1992 and 1997) are selected, which are circled in Fig.
221 2(c). A wet year is defined as the year in which the precipitation is more than one
222 standard deviation above the average precipitation, and similarly, the precipitation in a
223 dry year is lower than a standard deviation range. Accordingly, the division of time
224 period also applies to the precipitation series of the dry and wet years. It is specifically
225 observed that the dry years are distributed in both two periods, with the average
226 precipitation of 17.15 and 18.34 mm mon⁻¹ before and after 1997, whereas the wet years
227 occur before 1997 with an average of 51.03 mm mon⁻¹ but disappear after 1997.

228 3.2 Changes in summer precipitation shed and regional contributions

229 From 1980 to 2019, the average value of the IP summer precipitation is about
230 30.64 mm mon⁻¹. More than 93 % of this summer precipitation has been tracked by the
231 global surface through modelling, averaging 28.53 mm mon⁻¹. The climatology of the
232 moisture contribution during the 40 years is shown in Fig. 4 (a). The moisture
233 contribution to the IP generally decreases as its distance to IP increases. Although the
234 precipitation shed of the IP summer precipitation is global in scope, the contribution of
235 the area far away is negligible to be considered. Therefore, the 90th precipitation shed

236 enclosed by the black line in Fig. 4 is given full attention as the main moisture source
237 region in the following text. The main moisture source of the IP covers not only the
238 local grids in the study region, but also several of non-local land and oceanic areas. Due
239 to the dominance of the westerlies in the tropical–subtropical North Atlantic corridor
240 (Gimeno et al., 2010), most of the non-local source grids are located in the North
241 American land and the North Atlantic Ocean west of the study area, which jointly form
242 a relatively stable atmospheric basin in the global atmospheric moisture networks
243 (Zhang et al., 2020) under the influence of the summer anticyclonic structure (Fig. 4(a)).
244 The other source grids are located east of the North Atlantic Ocean and the IP, which is
245 the downwind zone for water vapor transport, covering Western Europe and the
246 Mediterranean. These eastern regions with positive atmospheric moisture divergence
247 provide a net water flux to the atmosphere, moisten the air parcels flowing towards the
248 surrounding land, and become the main short-term moisture sources affecting the IP,
249 especially the eastern IP (Gimeno et al., 2010; Vázquez et al., 2020). Hence, the main
250 moisture sources are divided into the three partial regions of the local IP, the west and
251 the east by the boundary of the study area and the eastern boundary of the Atlantic
252 Ocean (red and blue lines in Fig. 4), and the contribution of each region to the IP
253 precipitation can be quantified and compared.



254

255 **Figure 4** (a) Climatological 90th precipitation shed of the IP sink region and moisture contribution
 256 to the IP summer precipitation from 1980 to 2019. The black outlines show the 90th precipitation shed
 257 boundary during the 40 years. The vectors represent the climatological monthly water vapor flux.
 258 The red line encloses the study area, and the blue line divides the precipitation shed excluding the IP
 259 into the west (left area) and the east (right area) regions. (b) Differences in the moisture contribution
 260 in the 90th precipitation shed between 1998-2019 and 1980-1997 (average of 1998-2019 minus
 261 average of 1980-1997). The dots indicate 0.1 significance of the difference.

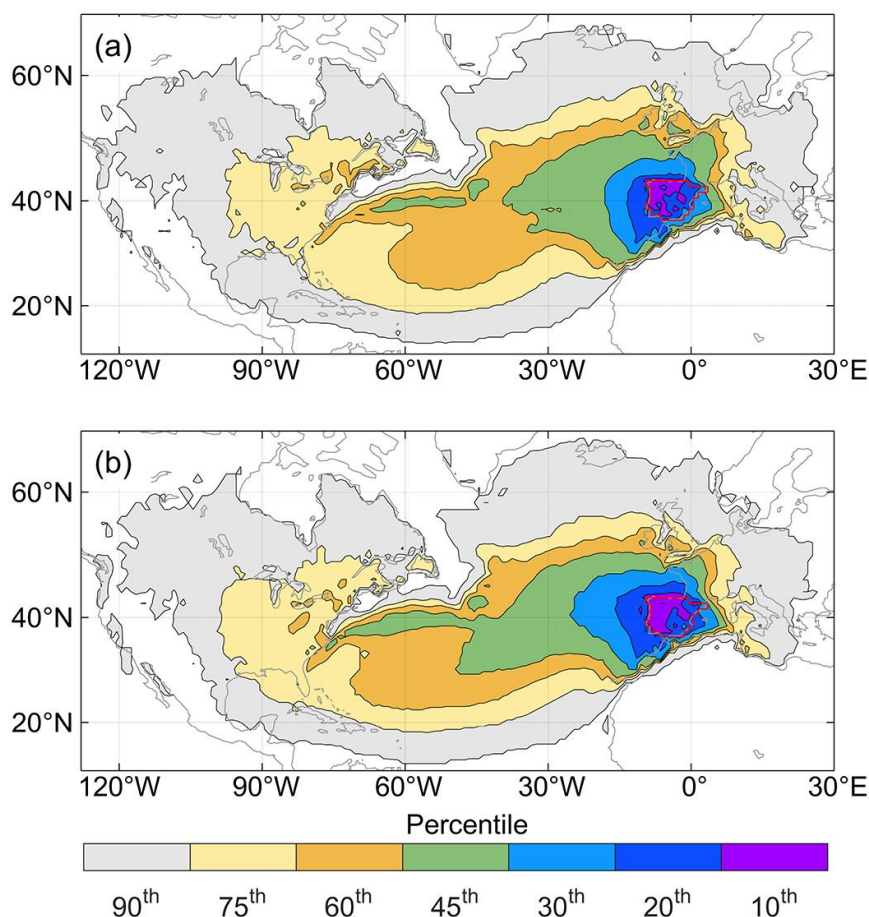
262 Affected by the transport distance, the grids with high contribution are located in
 263 and around the target IP region, with the maximum values for grids in the northwest

264 corner of the IP. The local IP contributes 3.46 mm mon^{-1} average summer precipitation,
265 with the precipitation recycling ratio of around 13.26 % during the 40 years. The west,
266 as the largest subregion of the precipitationshed, contributes the most summer
267 precipitation of $19.38 \text{ mm mon}^{-1}$ and occupies 76.06 % of the tracked precipitation
268 averagely. While the east region, which is in an unfavorable downwind position in the
269 summer circulation, provides only 2.81 mm mon^{-1} summer precipitation, accounting
270 for 10.68 %.

271 The difference in moisture contribution obtained from the 1998-2019 period minus
272 the 1980-1997 period is shown in Fig. 4(b). Almost all grid contributions show a
273 decrease after 1997. The grids with a large moisture contribution decline are mainly
274 concentrated in the IP, with the maximum reduction exceeding an average of 3 mm
275 mon^{-1} (more than 50% of its climatological moisture contribution). Compared with
276 other non-local source grids, the grids with higher contributions along the east coast of
277 the North Atlantic near the IP also have a slight but significant reduction in contribution.

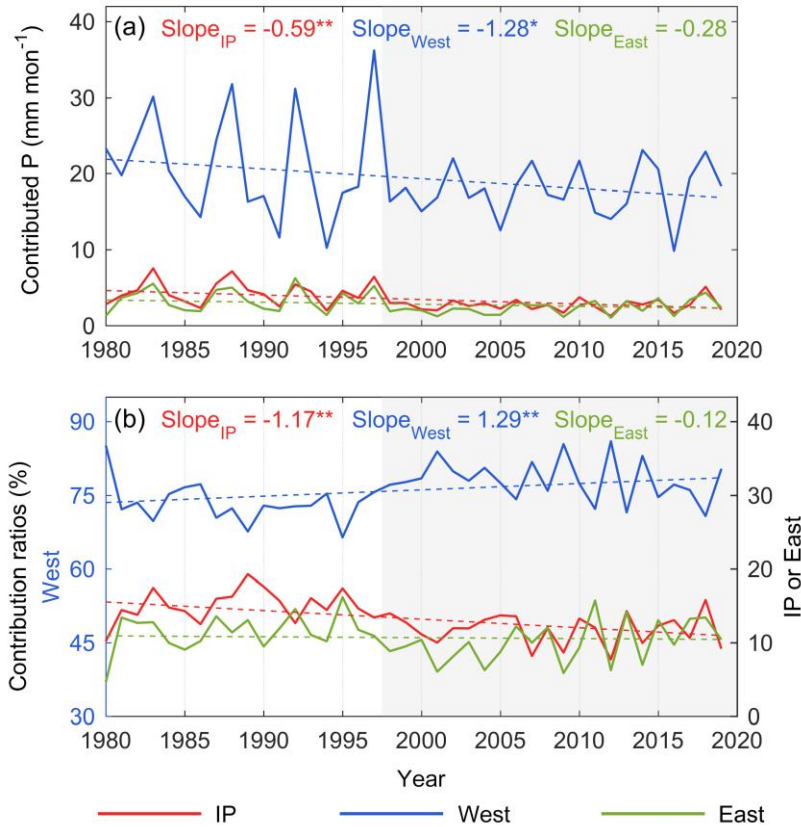
278 Due to the uneven distribution of grid contribution reduction in space, the area of
279 different percentile precipitationsheds differs in the two periods. The areas with
280 different colors in the distribution map of Fig. 5 represent the precipitationshed
281 boundaries at different percentiles in the two periods. During 1998-2019, the
282 precipitationshed boundary of each percentile extends westward in varying degrees
283 compared with those before 1997. The top decile of the contribution is still in the
284 western half of the IP. In the North Atlantic, the westward expansion of the western

285 boundary of the precipitationsheds is conspicuous, especially the 45th and 60th
 286 percentile precipitationsheds shown in orange and green color in Fig. 5(a, b). This
 287 westward extension implies that the significant and substantial reduction in the
 288 contribution of the local grids and its surrounding grids results in a decrease in the
 289 proportion of these areas. Therefore, for the same percentile of the precipitationshed,
 290 only a smaller area concentrated by high-contribution grids is sufficient before 1997.
 291 However, a larger area is required for the same proportion after 1997.



292
 293 **Figure 5** Different percentile precipitationsheds during the two periods (a) 1980-1997 and (b) 1998-
 294 2019. The proportion of the cumulative contribution to the IP precipitation from all areas enclosed
 295 by the contour line is the percentile indicated by the corresponding color.

296 Figure 6(a) shows the quantified precipitation contributed by the local IP, the west
297 and the east regions. The negative slopes in Fig. 6(a) indicate that the summer
298 precipitation contributed by these three regions has a downward trend, especially
299 significant for the IP and the west with slopes of -0.59 and $-1.28 \text{ mm mon}^{-1} \text{ decade}^{-1}$.
300 These decreasing trends cause a 6.38 mm mon^{-1} difference in precipitation from the
301 main source region in the two periods, which explains 82.64% of the total reduction in
302 the IP summer precipitation (7.72 mm mon^{-1}). In terms of the difference in the average
303 values of each region, the precipitation contributed by the local IP, the west and the east
304 significantly decreases from 4.38 , 21.37 and 3.41 mm mon^{-1} in 1980-1997 to 2.71 ,
305 17.76 and 2.32 mm mon^{-1} in 1998-2019, respectively. 26.32% , 56.53% and 17.15%
306 of the difference in the main source supply between the two periods are due to the
307 contribution decline from the local IP, the west and the east, respectively.



308

309 **Figure 6** Variations of (a) contributed precipitation (unit of the slope: mm mon⁻¹ decade⁻¹) and (b)

310 contribution ratios (unit of the slope: % decade⁻¹) from the IP, the west and the east region during

311 1980-2019 summer. ‘***’ and ‘**’ represent 0.05 and 0.1 level significance of the trend.

312 The variation and trend of the contribution ratio of each region are shown in Fig.

313 6(b). The proportion of contributions from the local IP and the east shows a decreasing

314 trend throughout the 40 years with the slope of -1.17 % decade⁻¹ and -0.12 % decade⁻¹,

315 which is consistent with the decreasing trends of their absolute contributions.

316 Conversely, although the precipitation contributed by the west shows a decreasing trend,

317 its proportion is significantly increasing and the slope is 1.29 % decade⁻¹. The average

318 contribution ratios of the local IP and the east decrease from 15.05 % and 11.49 %

319 before 1997 to 11.79 % and 10.02 % after 1997, while the ratio of the west increases

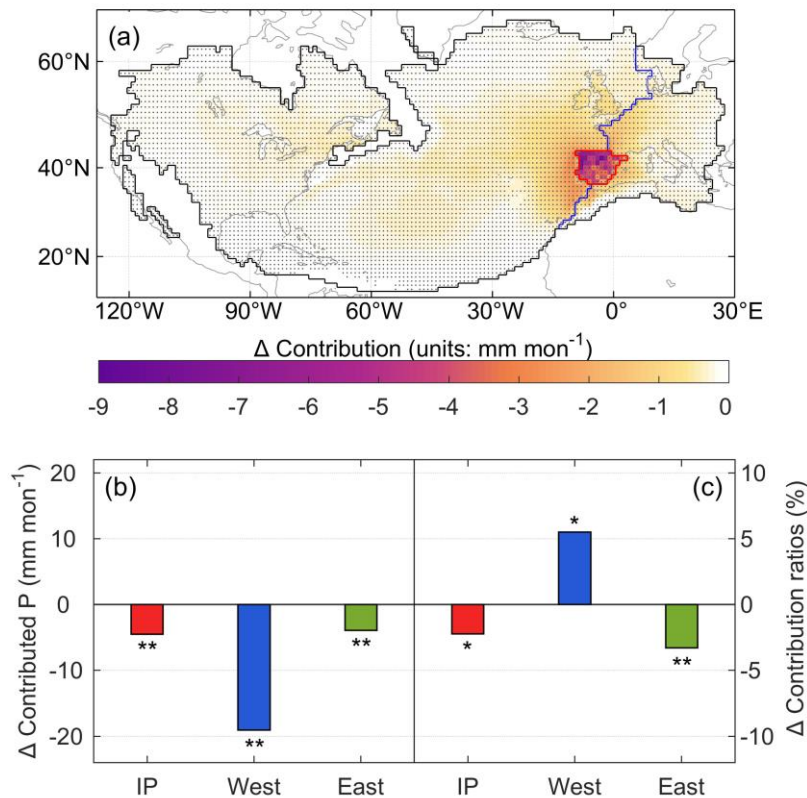
320 from 73.46 % to 78.19 %.

321 3.3 Differences in wet years and dry years

322 The dry years (1991, 1994, 2005, 2012 and 2016) and the wet years (1983 1987
323 1988 1992 and 1997) are selected as described in section 3.1. Of the two divided periods,
324 all the wet years only occur before 1997, while the dry years are distributed in both
325 periods with no decrease in its average value. This represents that although the average
326 summer precipitation after 1997 is reduced significantly compared with the previous
327 period, there is no decrease in the valley value of the precipitation series. Thus, the
328 disappearance of the wet years during 1998-2019 caused by the decrease of the
329 precipitation series peaks directly reflects the recent decrease in the IP summer
330 precipitation.

331 During the entire 40 years, differences in moisture contribution within the 90th
332 precipitation shed of the IP summer precipitation between the wet and dry years are
333 shown in Fig. 7(a). In the dry years, the significant reduction in the moisture
334 contribution from all grids in the main source region induces much lower precipitation
335 than in the wet years. On the grid scale, the larger declines primarily happened in the
336 local IP, and the grids with the largest drop, close to 9 mm mon⁻¹, are mainly
337 concentrated in the west and the north of the IP. In each source region, an average of
338 6.41, 30.74 and 5.34 mm mon⁻¹ of the summer IP precipitation is provided from the
339 local IP, the west and the east in the wet years, with 15.15 % recycling ratio, 72.19 %

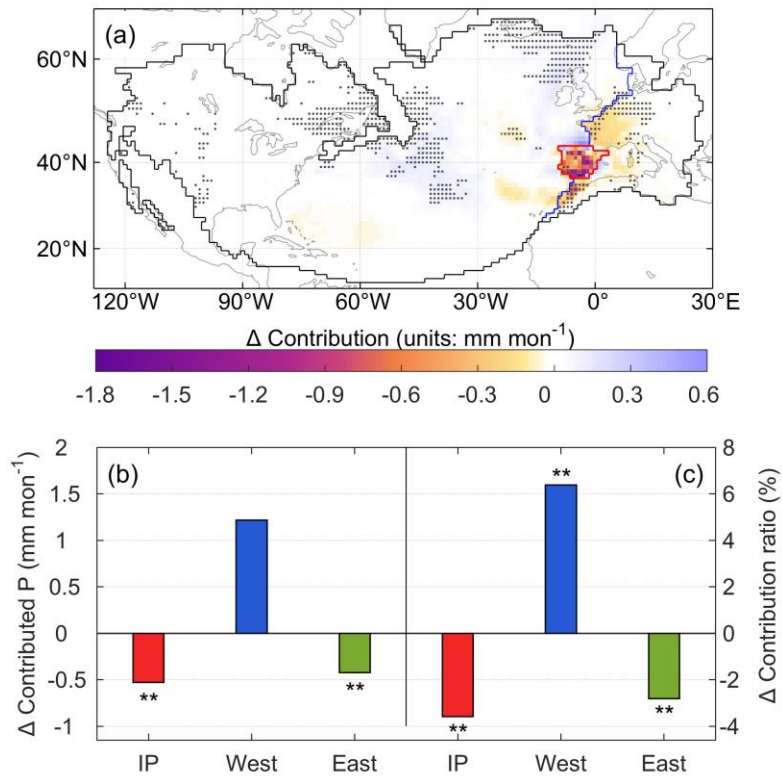
340 and 12.66 % contribution ratio. While in the dry years, the average precipitation
 341 contributed from each region is 1.92, 11.66 and 1.40 mm mon⁻¹, accounting for 12.93 %,
 342 77.70 % and 9.37 %, respectively. All three regions contribute more to summer
 343 precipitation in the wet years than in the dry years, and compared with the dry years,
 344 the contribution ratios of the local IP and the east in the wet years are also higher. The
 345 disappearance of the wet years after 1997, compared with those before 1997,
 346 exacerbates the decline in contributions from all three sources, due to the high moisture
 347 supply in the wet years. The decrease in the frequency of the wet years with higher local
 348 moisture recycling ratio and higher contribution ratio of the east leads to an increase in
 349 the proportion of the summer precipitation originating from the remaining other region,
 350 namely the west, during the same period.



351

352 **Figure 7** (a) Differences in the moisture contribution in the 90th precipitation shed between the dry
353 years and the wet years (average of the dry years minus average of the wet years). The dots indicate
354 0.1 significance of the difference. The changes in (b) average precipitation contributed from each
355 region and (c) their average contribution ratios between the dry years and the wet years. ‘***’ and ‘*’
356 represent 0.05 and 0.1 level significance of the difference.

357 The dry years in the two periods have been divided and compared with each other,
358 and the differences between the two periods are shown in Fig. 8. From the distribution
359 of differences, the grids with reduced moisture contribution are mainly located in the
360 IP and the east region, and the southern part of the IP has the largest decrease (Fig. 8(a)).
361 Mainly dominated by these negatively changing grids, both the absolute contribution
362 and the contribution ratio of the local IP and the east have dropped significantly, with
363 0.53 and 0.42 mm mon⁻¹ decrease in contributed precipitation and 3.58 % and 2.81 %
364 contribution ratio reduction, respectively (Fig. 8(b, c)). For the west region, however,
365 it raises the moisture contribution to the summer precipitation by 1.22 mm mon⁻¹ in the
366 dry years after 1997, causing a 6.39 % increase in its contribution ratio. Despite the dry
367 years with no decrease precipitation between the two periods, the decrease in the local
368 moisture recycling is still noticeable.



369

370 **Figure 8** (a) Differences in the moisture contribution in the 90th precipitation shed in the dry years
 371 between 1998-2019 and 1980-1997 (average of 1998-2019 minus average of 1980-1997). The dots
 372 indicate 0.1 significance of the difference. The changes in (b) average precipitation contributed from
 373 each region and (c) their average contribution ratios in the dry years between 1998-2019 and 1980-
 374 1997. ‘***’ and ‘**’ represent 0.05 and 0.1 level significance of the difference.

375 4. Discussion

376 The trends in the contribution from the three source regions, the local, the west
 377 and the east regions, to all seasonal and annual precipitation over the past 40 years are
 378 listed in Table 1. In general, the decreasing trend maintained by the local IP and the east
 379 region are closely related to the drought in the Mediterranean basin (Ribeiro et al., 2020;
 380 Russo et al., 2019), and the increasing proportion of the west can be explained by the

381 increasingly important role of the oceanic moisture in terrestrial precipitation (Gimeno
382 et al., 2020; Vicente-Serrano et al., 2018). The simultaneous decrease in the moisture
383 contribution from all three regions is responsible for the significant decrease in only the
384 summer precipitation series among all seasonal or annual precipitation. In particular,
385 the local moisture recycling ratio in summer is obviously way down, differentiating the
386 reduced summer precipitation from the other seasons. It is worth highlighting that this
387 significant decrease in recent summer precipitation over the IP in this study is based on
388 a short record (1980-2019) from ERA5, while a long-term assessment of precipitation
389 (1850-2018) from multiple sources still lacks a statistically significant decreasing trend
390 (Peña-Angulo et al., 2020). Nevertheless, the changes in the recent four decades still
391 show the significant influence of the local moisture recycling, especially on the trend
392 of summer precipitation and variation of summer wet and dry years.

393

394 **Table 1** Trends of contributions from the IP, the west and the east to annual and seasonal
395 precipitation, and the trends of their contribution ratios.

	Contributed precipitation (mm mon ⁻¹ decade ⁻¹)					Contribution ratio (% decade ⁻¹)				
	Annual	Spring	Summer	Autumn	Winter	Annual	Spring	Summer	Autumn	Winter
IP	-0.24**	-0.30	-0.59**	-0.03	-0.03	-0.49**	-0.66**	-1.17**	-0.14	-0.08
West	0.53	1.67	-1.28*	1.23	0.52	0.81**	0.80	1.29**	0.38	0.77
East	-0.17	-0.06	-0.28	-0.05	-0.29	-0.32	-0.14	-0.12	-0.24	-0.69

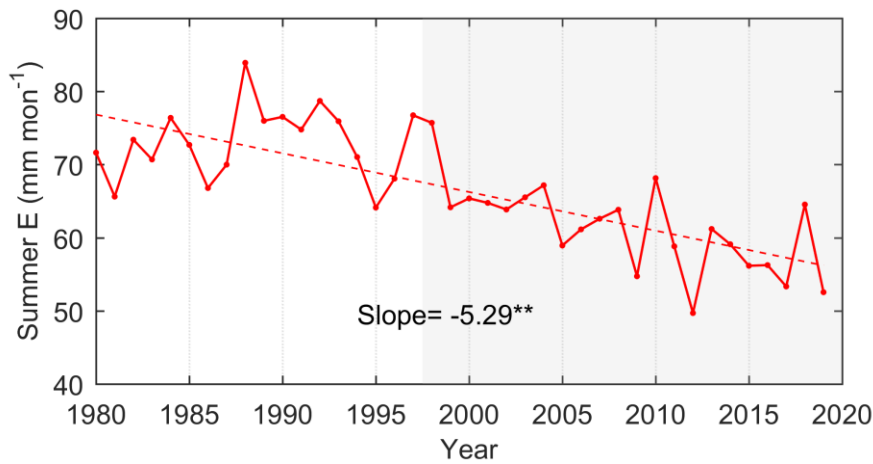
396 ‘**’ and ‘*’ represent 0.05 and 0.1 level significance of the trend.

397 The remarkable decrement of summer precipitation can be attributed to the

398 simultaneous and large reduction of contributions from all three source regions.
399 Moisture transport from the west region contributing to the IP precipitation is mainly
400 through the tropical–subtropical North Atlantic corridor. In summer, air masses from
401 the west in this transportation process, as it gets closer to the destination, gradually shift
402 from a net supply to a net uptake of the IP precipitation (Gimeno et al., 2010). In this
403 case, the stronger land-sea contrast caused by the warming land surface makes the
404 advected air mass from the Atlantic experience more drying and a decrease in the
405 contribution from the west (Cramer et al., 2018; Kröner et al., 2017). In addition, the
406 extension of Hadley circulation makes the IP more strongly affected by subsidence,
407 generating higher static stability (Brogli et al., 2019). This results in a lower frequency
408 of extreme heavy precipitation characterized by the presence of a cutoff low at mid-
409 levels and an easterly moisture flow from the Mediterranean Sea (Merino et al., 2016).
410 However, the ocean warming patterns and thermodynamics can promote precipitation
411 in cold seasons (Brogli et al., 2019), just as shown by the increasing contributed
412 precipitation from the west in autumn and winter in Table 1. It suggests the drivers
413 leading to less summer precipitation do not generally cause a similar change in the
414 precipitation in the other seasons.

415 In terms of the total contribution from the three subregions, the west region
416 dominates more of the reduction in the IP precipitation due to its wide coverage with a
417 large number of grids. Nevertheless, in the local IP, which is much smaller than the
418 west, the high contribution per grid, the difference between the two periods, and the

419 consistent decline of the precipitation recycling ratio make the role of the local
420 contribution variation worth emphasizing. As an important indicator to describe the
421 interaction between the surface and atmospheric processes, the change in the
422 precipitation recycling ratio takes into account changes in both precipitation and the
423 contribution of local evaporation (Goessling and Reick, 2011; Zhang, 2020). For the IP,
424 its significant reduction in local moisture contribution is most likely due to the
425 weakening of local evaporation (Fig. 9), with a correlation coefficient of 0.64 between
426 evaporation and the locally contributed precipitation. In summer, soil moisture and the
427 recycling process driven by evaporation are regarded as an active source of moisture
428 (Jung et al., 2010; Vicente-Serrano et al., 2014), leading to a positive correlation
429 between soil moisture and precipitation. As a result, during those dry summers, the
430 declining precipitation causes the shortage of soil water supply, the limitation of soil
431 water evaporation capacity and the consequent reduction in surface evaporation
432 (García-Valdecasas Ojeda et al., 2020; Ruosteenoja et al., 2018). The IP precipitation
433 can be further reduced due to this weakening of the local moisture recycling. This
434 continuous feedback of the interactions of soil moisture evaporation and precipitation
435 can exacerbate the water resource depletion and summer drought, especially in dry
436 years. Thus, despite the ongoing emphasis on the significance of the ocean as a moisture
437 source, consistent changes in the local moisture contribution or proportion with reduced
438 precipitation require more attention.



439

440 **Figure 9** Time series of the IP summer evaporation from the ERA5 during 1980-2019 (unit of the
 441 slope: mm mon⁻¹ decade⁻¹). ‘***’ represents 0.05 level significance of the trend.

442 5. Conclusions

443 Decreasing summer precipitation over the IP could lead to an escalation of drought,
 444 especially with the high temperature and low rainfall characteristics of Mediterranean
 445 climate. In this study, using the reanalysis data ERA5 and WAM-2layers model, we
 446 investigated how changes in moisture contribution from the sources, including the IP,
 447 the west and the east, affect the reduction in summer precipitation between 1980-1997
 448 and 1998-2019. The major findings attribute the decreasing precipitation to the changes
 449 in moisture contribution at sources and highlight their importance, which are
 450 summarized below.

451 1) The reduction of contribution to IP summer precipitation is mainly concentrated in
 452 the IP and its neighboring grids. The local IP grids show the greatest reduction, and
 453 the surrounding grids show a slight but significant decrease.

454 2) Compared with the summer of 1980-1997, the IP and the east contributed 1.7 and

455 1.1 mm mon⁻¹ less IP precipitation during 1998-2019, accounting for 26% and 17%
456 of the main source supply reduction, respectively. Meanwhile, the importance of
457 the vast west region was clearly shown by reducing the IP precipitation by 3.6 mm
458 mon⁻¹, representing 57% of the decrease in precipitation originating from main
459 sources.

460 3) The contributions from the local IP and the east keep declining during the 40 years.
461 In particular, the significant reduction in the local moisture recycling, reflected in
462 the disappearance of the wet years after 1997 and the reduction of local
463 contributions in the dry years, suggests a close link with the decrease in summer
464 precipitation.

465

466 **Code and Data availability**

467 Code and data used in this manuscript are available from the corresponding author upon
468 a reasonable request.

469

470 **Author contributions**

471 MG and QT designed the study; YL performed the analysis and calculation; CZ
472 contributed to the application of the model in this study; YL prepared the manuscript
473 draft, and all co-authors reviewed and edited the manuscript.

474

475 **Competing interests**

476 The authors declare no competing interests.

477

478 **Acknowledgements**

479 This study was partly funded by the National Natural Science Foundation of China

480 (41730645 and 41701033) and the Strategic Priority Research Program of Chinese

481 Academy of Sciences (XDA20060402). The authors would like to thank the EU and

482 Innovation Fund Denmark (IFD) for funding within the framework of the FORWARD

483 collaborative international consortium financed through the ERA-NET co-fund

484 WaterWorks2015 integral part of the 2016 joint activities developed by the “Water

485 Challenges for a Changing World” joint programme initiative (Water JPI).

486

487 **References**

- 488 Boé, J., and Terray, L.: Land–sea contrast, soil-atmosphere and cloud-temperature
489 interactions: interplays and roles in future summer European climate change,
490 *Clim. Dyn.*, 42, 683-699, <https://doi.org/10.1007/s00382-013-1868-8>, 2014.
- 491 Boé, J., Terray, L., Cassou, C., and Najac, J.: Uncertainties in European summer
492 precipitation changes: role of large scale circulation, *Clim. Dyn.*, 33, 265-276,
493 <https://doi.org/10.1007/s00382-008-0474-7>, 2009.
- 494 Bonne, J. L., Masson-Delmotte, V., Cattani, O., Delmotte, M., and Steen-Larsen, H. C.:
495 The isotopic composition of water vapour and precipitation in Ivittuut, Southern
496 Greenland, *Atmos. Chem. Phys.*, 14, 4419-2014, <https://doi.org/10.5194/acp-14-4419-2014>, 2014.
- 498 Brogli, R., Sørland, S. L., Kröner, N., and Schär, C.: Causes of future Mediterranean
499 precipitation decline depend on the season, *Environ. Res. Lett.*, 14, 114017,
500 <https://doi.org/10.1088/1748-9326/ab4438>, 2019.
- 501 Burde, G. I.: Bulk recycling models with incomplete vertical mixing. Part I: Conceptual
502 framework and models, *J. Clim.*, 19, 1461-1472,
503 <https://doi.org/10.1175/jcli3687.1>, 2010.
- 504 Cortesi, N., Trigo, R. M., Gonzalez-Hidalgo, J. C., and Ramos, A. M.: Modeling
505 monthly precipitation with circulation weather types for a dense network of
506 stations over Iberia, *Hydrol. Earth Syst. Sci.*, 17, 665-678,
507 <https://doi.org/10.5194/hess-17-665-2013>, 2013.
- 508 Cramer, W., Guiot, J., Fader, M., Garrabou, J., Gattuso, J.-P., Iglesias, A., . . . Xoplaki,
509 E.: Climate change and interconnected risks to sustainable development in the
510 Mediterranean, *Nat. Clim. Chang.*, 8, 972-980, <https://doi.org/10.1038/s41558-018-0299-2>, 2018.
- 512 Damián, I.-C., and Gonzalo, M. M.: A new moisture tagging capability in the Weather
513 Research and Forecasting model: formulation, validation and application to the
514 2014 Great Lake-effect snowstorm, *Earth Syst. Dynam.*, 9, 167-185,
515 <https://doi.org/10.5194/esd-9-167-2018>, 2018.
- 516 García-Valdecasas Ojeda, M., Yeste, P., Gámiz-Fortis, S. R., Castro-Díez, Y., and
517 Esteban-Parra, M. J.: Future changes in land and atmospheric variables: An
518 analysis of their couplings in the Iberian Peninsula, *Sci. Total Environ.*, 722,
519 137902, <https://doi.org/10.1016/j.scitotenv.2020.137902>, 2020.
- 520 Gimeno, L., Nieto, R., and Sorí, R.: The growing importance of oceanic moisture
521 sources for continental precipitation, *npj Clim. Atmos. Sci.*, 3, 27,
522 <https://doi.org/10.1038/s41612-020-00133-y>, 2020.
- 523 Gimeno, L., Nieto, R., Trigo, R. M., Vicente-Serrano, S. M., and López-Moreno, J. I.:
524 Where does the Iberian Peninsula moisture come from? An answer based on a
525 Lagrangian approach, *J. Hydrometeorol.*, 11, 421-436,
526 <https://doi.org/10.1175/2009JHM1182.1>, 2010.

527 Goessling, H. F., and Reick, C. H.: What do moisture recycling estimates tell us?
528 Exploring the extreme case of non-evaporating continents, *Hydrol. Earth Syst.*
529 *Sci.*, 15, 3217-3235, <https://doi.org/10.5194/hess-15-3217-2011>, 2011.

530 Goessling, H. F., and Reick, C. H.: On the "well-mixed" assumption and numerical 2-
531 D tracing of atmospheric moisture, *Atmos. Chem. Phys.*, 13, 5567-5585,
532 <https://doi.org/10.5194/acp-13-5567-2013>, 2013.

533 Herrera, S., Cardoso, R. M., Soares, P. M., Espírito-Santo, F., and Gutiérrez, J.: Iberia01:
534 a new gridded dataset of daily precipitation and temperatures over Iberia, *Earth*
535 *Syst. Sci. Data*, 11, 1947-1956, <https://doi.org/10.5194/essd-11-1947-2019>,
536 2019.

537 Hersbach, H., Bell, B., Berrisford, P., Hirahara, S., Horányi, A., Muñoz-Sabater, J., . . .
538 Thépaut, J.-N.: The ERA5 global reanalysis, *Quarterly Journal of the Royal*
539 *Meteorological Society*, 146, 1999-2049, <https://doi.org/10.1002/qj.3803>, 2020.

540 Jung, M., Reichstein, M., Ciais, P., Seneviratne, S. I., Sheffield, J., Goulden, M. L., . . .
541 Zhang, K.: Recent decline in the global land evapotranspiration trend due to
542 limited moisture supply, *Nature*, 467, 951-954,
543 <https://doi.org/10.1038/nature09396>, 2010.

544 Keys, P. W., Barnes, E. A., van der Ent, R. J., and Gordon, L. J.: Variability of moisture
545 recycling using a precipitationshed framework, *Hydrology and Earth System*
546 *Sciences*, 18, 3937-3950, <https://doi.org/10.5194/hess-18-3937-2014>, 2014.

547 Keys, P. W., Ent, R., Gordon, L. J., Hoff, H., and Savenije, H.: Analyzing
548 precipitationsheds to understand the vulnerability of rainfall dependent regions,
549 *Biogeosciences Discussions*, 8, 2011.

550 Kröner, N., Kotlarski, S., Fischer, E., Lüthi, D., Zubler, E., and Schär, C.: Separating
551 climate change signals into thermodynamic, lapse-rate and circulation effects:
552 theory and application to the European summer climate, *Clim. Dyn.*, 48, 3425-
553 3440, <https://doi.org/10.1007/s00382-016-3276-3>, 2017.

554 Lenderink, G., van Ulden, A., van den Hurk, B., and van Meijgaard, E.: Summertime
555 inter-annual temperature variability in an ensemble of regional model
556 simulations: analysis of the surface energy budget, *Clim. Change*, 81, 233-247,
557 <https://doi.org/10.1007/s10584-006-9229-9>, 2007.

558 Lopez-Bustins, J. A., and Lemus-Canovas, M.: The influence of the Western
559 Mediterranean Oscillation upon the spatio-temporal variability of precipitation
560 over Catalonia (northeastern of the Iberian Peninsula), *Atmos. Res.*, 236,
561 104819, <https://doi.org/10.1016/j.atmosres.2019.104819>, 2020.

562 Maasch, K. A.: Statistical detection of the mid-Pleistocene transition, *Climate*
563 *Dynamics*, 2, 133-143, <https://doi.org/10.1007/BF01053471>, 1988.

564 Merino, A., Fernández-Vaquero, M., López, L., Fernández-González, S., Hermida, L.,
565 Sánchez, J. L., . . . Gascón, E.: Large-scale patterns of daily precipitation
566 extremes on the Iberian Peninsula, *International Journal of Climatology*, 36,
567 3873-3891, <https://doi.org/https://doi.org/10.1002/joc.4601>, 2016.

568 Numaguti, A.: Origin and recycling processes of precipitating water over the Eurasian
569 continent: Experiments using an atmospheric general circulation model, *J.*
570 *Geophys. Res.-Atmos.*, 104, 1957-1972,
571 <https://doi.org/10.1029/1998JD200026>, 1999.

572 Páscoa, P., Russo, A., Gouveia, C. M., Soares, P. M. M., Cardoso, R. M., Careto, J. A.
573 M., and Ribeiro, A. F. S.: A high-resolution view of the recent drought trends
574 over the Iberian Peninsula, *Weather Clim. Extremes*, 32, 100320,
575 <https://doi.org/10.1016/j.wace.2021.100320>, 2021.

576 Peña-Angulo, D., Vicente-Serrano, S. M., Domínguez-Castro, F., Murphy, C., Reig, F.,
577 Trambly, Y., . . . El Kenawy, A.: Long-term precipitation in Southwestern
578 Europe reveals no clear trend attributable to anthropogenic forcing, *Environ.*
579 *Res. Lett.*, 15, 094070, <https://doi.org/10.1088/1748-9326/ab9c4f>, 2020.

580 Rajczak, J., and Schär, C.: Projections of future precipitation extremes over Europe: A
581 multimodel assessment of climate simulations, *J. Geophys. Res.-Atmos.*, 122,
582 10,773-710,800, <https://doi.org/10.1002/2017JD027176>, 2017.

583 Ribeiro, A. F. S., Russo, A., Gouveia, C. M., and Pires, C. A. L.: Drought-related hot
584 summers: A joint probability analysis in the Iberian Peninsula, *Weather Clim.*
585 *Extremes*, 30, 100279, <https://doi.org/10.1016/j.wace.2020.100279>, 2020.

586 Ruosteenoja, K., Markkanen, T., Venäläinen, A., Räisänen, P., and Peltola, H.: Seasonal
587 soil moisture and drought occurrence in Europe in CMIP5 projections for the
588 21st century, *Clim. Dyn.*, 50, 1177-1192, [https://doi.org/10.1007/s00382-017-](https://doi.org/10.1007/s00382-017-3671-4)
589 [3671-4](https://doi.org/10.1007/s00382-017-3671-4), 2018.

590 Russo, A., Gouveia, C. M., Dutra, E., Soares, P. M. M., and Trigo, R. M.: The synergy
591 between drought and extremely hot summers in the Mediterranean, *Environ.*
592 *Res. Lett.*, 14, 014011, <https://doi.org/10.1088/1748-9326/aaf09e>, 2019.

593 Serrano, A., García, J. A., Mateos, V. L., Cancillo, M. L., and Garrido, J.: Monthly
594 modes of variation of precipitation over the Iberian Peninsula, *J. Clim.*, 12,
595 2894-2919, 1999.

596 Stohl, A., and James, P.: A Lagrangian analysis of the atmospheric branch of the global
597 water cycle. Part I: Method description, validation, and demonstration for the
598 August 2002 flooding in Central Europe, *J. Hydrometeorol.*, 5, 656, 2004.

599 Stohl, A., and James, P.: A Lagrangian analysis of the atmospheric branch of the global
600 water cycle. Part II: Moisture transports between earth's ocean basins and river
601 catchments, *J. Hydrometeorol.*, 6, 961-984, <https://doi.org/10.1175/JHM470.1>,
602 2005.

603 Tang, Q., Leng, G., and Groisman, P. Y.: European hot summers associated with a
604 reduction of cloudiness, *J. Clim.*, 25, 3637-3644, [https://doi.org/10.1175/JCLI-](https://doi.org/10.1175/JCLI-D-12-00040.1)
605 [D-12-00040.1](https://doi.org/10.1175/JCLI-D-12-00040.1), 2012.

606 Teuling, A. J., Van Loon, A. F., Seneviratne, S. I., Lehner, I., Aubinet, M., Heinesch,
607 B., . . . Spank, U.: Evapotranspiration amplifies European summer drought,
608 *Geophys. Res. Lett.*, 40, 2071-2075, <https://doi.org/10.1002/grl.50495>, 2013.

609 Ulbrich, U., Christoph, M., Pinto, J. G., and Corte-Real, J.: Dependence of winter
610 precipitation over Portugal on NAO and baroclinic wave activity, *International*
611 *Journal of Climatology*, 19, 379-390, [https://doi.org/10.1002/\(SICI\)1097-0088\(19990330\)19:4<379::AID-JOC357>3.0.CO;2-8](https://doi.org/10.1002/(SICI)1097-0088(19990330)19:4<379::AID-JOC357>3.0.CO;2-8), 2015.

612
613 van der Ent, R. J., and Savenije, H. H. G.: Length and time scales of atmospheric
614 moisture recycling, *Atmos. Chem. Phys.*, 11, 1853-1863,
615 <https://doi.org/10.5194/acp-11-1853-2011>, 2011.

616 van der Ent, R. J., Savenije, H. H. G., Schaeffli, B., and Steele-Dunne, S. C.: Origin and
617 fate of atmospheric moisture over continents, *Water Resour. Res.*, 46,
618 <https://doi.org/10.1029/2010WR009127>, 2010.

619 van der Ent, R. J., Tuinenburg, O. A., Knoche, H. R., Kunstmann, H., and Savenije, H.
620 H. G.: Should we use a simple or complex model for moisture recycling and
621 atmospheric moisture tracking?, *Hydrol. Earth Syst. Sci.*, 17, 4869-4884,
622 <https://doi.org/10.5194/hess-17-4869-2013>, 2013.

623 van der Ent, R. J., Wang-Erlandsson, L., Keys, P., and Savenije, H.: Contrasting roles
624 of interception and transpiration in the hydrological cycle - Part 2: Moisture
625 recycling, *Earth Syst. Dynam.*, 5, <https://doi.org/10.5194/esdd-5-281-2014>,
626 2014.

627 Vázquez, M., Nieto, R., Liberato, M. L. R., and Gimeno, L.: Atmospheric moisture
628 sources associated with extreme precipitation during the peak precipitation
629 month, *Weather and Climate Extremes*, 30, 100289,
630 <https://doi.org/https://doi.org/10.1016/j.wace.2020.100289>, 2020.

631 Vicente-Serrano, S. M., Azorin-Molina, C., Sanchez-Lorenzo, A., Morán-Tejeda, E.,
632 Lorenzo-Lacruz, J., Revuelto, J., . . . Espejo, F.: Temporal evolution of surface
633 humidity in Spain: recent trends and possible physical mechanisms, *Clim. Dyn.*,
634 42, 2655-2674, <https://doi.org/10.1007/s00382-013-1885-7>, 2014.

635 Vicente-Serrano, S. M., Nieto, R., Gimeno, L., Azorin-Molina, C., Drumond, A., El
636 Kenawy, A., . . . Peña-Gallardo, M.: Recent changes of relative humidity:
637 regional connections with land and ocean processes, *Earth Syst. Dynam.*, 9,
638 915-937, <https://doi.org/10.5194/esd-9-915-2018>, 2018.

639 Zhang, C.: Moisture source assessment and the varying characteristics for the Tibetan
640 Plateau precipitation using TRMM, *Environ. Res. Lett.*, 15, 104003,
641 <https://doi.org/10.1088/1748-9326/abac78>, 2020.

642 Zhang, C., Tang, Q., and Chen, D.: Recent changes in the moisture source of
643 precipitation over the Tibetan Plateau, *J. Clim.*, 30, 1807-1819,
644 <https://doi.org/10.1175/JCLI-D-15-0842.1>, 2017.

645 Zhang, Y., Huang, W., Zhang, M., Tian, Y., Wang, G., and Zhong, D.: Atmospheric
646 Basins: Identification of Quasi-Independent Spatial Patterns in the Global
647 Atmospheric Hydrological Cycle Via a Complex Network Approach, *J.*
648 *Geophys. Res.-Atmos.*, 125, e2020JD032796,
649 <https://doi.org/https://doi.org/10.1029/2020JD032796>, 2020.

650 Zhu, Y., and Newell, R. E.: A proposed algorithm for moisture fluxes from atmospheric
651 rivers, Mon. Weather Rev., 126, 725-735, [https://doi.org/10.1175/1520-0493\(1998\)126<0725:Apafmf>2.0.Co;2](https://doi.org/10.1175/1520-0493(1998)126<0725:Apafmf>2.0.Co;2), 1998.

653